

Quantized relativistic flux tube

Collin Olson and M. G. Olsson

Department of Physics, University of Wisconsin, Madison, Wisconsin 53706

Dan LaCourse

Department of Physics, Bethany College, Lindsborg, Kansas 67456

(Received 11 June 1993)

We explore the dynamics of mesons composed of spinless quarks connected by a straight flux tube. The mesons are quantized and the constituent motion is relativistic. The methods developed are applied to mesons containing equal mass quarks and heavy-light quarks. For massless quarks a nearly straight leading Regge trajectory with Nambu slope is accompanied by nearly parallel equally spaced daughter trajectories. For heavy-light mesons an analogous structure is found but with double the usual Nambu slope. Comparison with six observed spin-averaged heavy-light meson states yields good agreement.

PACS number(s): 12.38.Aw, 12.38.Lg

I. INTRODUCTION

The last few years have witnessed some rapid progress in understanding hadronic states on both experimental and theoretical fronts. In the arena of model building the relativistic flux tube (RFT) model has been proposed [1-3] as a successor to the potential model. As previously pointed out [2, 4], the spin-independent relativistic correction generated by a Lorentz scalar confining potential is inconsistent with QCD. In addition, the small quark mass limit with a scalar confinement potential implies a catastrophic loss of Regge behavior [5]. The Lorentz scalar nature of confinement has no obvious basis in fundamental QCD but was chosen phenomenologically [6] to avoid long range spin-spin correlations. Once this choice is made one must accept the spin-independent consequences. These consequences require the rejection of the concept of scalar confinement.

The RFT model gives, in a natural way, the correct spin dependence [3], the correct spin-independent corrections [2, 3], and for massless quarks reduces to the Nambu string. The RFT model also provides a simple physical picture for the QCD relativistic corrections derived from the rigorous Wilson loop formalism [4, 7]. The leading relativistic correction at large angular momentum is just due to the energy of the flux tube rotating about the c.m. of the heavy quarks [2]. The qualitative change introduced by the RFT model is to include the momentum of the interacting field whereas the potential model only includes its energy.

In [1] an effort was made to solve the spinless quark RFT model for quantized mesons. The purpose of the present work is to expand upon this treatment, to develop more accurate numerical procedures, and to explore the Regge structure of heavy-light mesons. The basic technical problem with the quantum solution is that one cannot analytically eliminate all of the quark velocities between the energy and angular momentum equations. We develop a systematic approach which efficiently handles quantum systems of this type. In Sec. II we generate the

equations of motion by the tube substitution approach [3] and discuss the classical *grast* solutions in the cases of equal mass quarks and heavy-light quarks. The quantum solution is outlined in Sec. III and some detailed numerical solutions are given in Sec. IV for equal mass quarks and in Sec. V for heavy-light systems. Our conclusions are summarized in Sec. VI. In the Appendix we present some analytic results for the operator representations used and discuss the convergence of our numerical procedure.

II. RFT EQUATIONS AND CLASSICAL SOLUTIONS

In Fig. 1 we show the portion of a meson from the meson c.m. to the *i*th quark including the corresponding portion of the flux tube. For the *i*th quark alone the free Hamiltonian is

$$H_{0i} = \sqrt{\mathbf{p}_{qi}^2 + m_i^2}. \tag{1}$$

The flux tube segment is introduced by a four-momentum substitution [3]

$$p_q^\mu \rightarrow p^\mu - p_i^\mu, \tag{2}$$

where p^μ is the new canonical momentum and

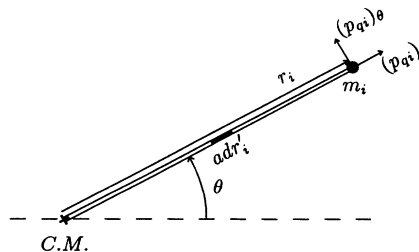


FIG. 1. Portion of a meson consisting of a segment of flux tube from the center of momentum to the *i*th quark.

$$p_i^\mu = (H_i, \mathbf{p}_i) \quad (3)$$

is the tube four-momentum. By direct evaluation [1, 2],

$$\begin{aligned} H_{ti} &= ar_i \frac{\arcsin v_{\perp i}}{v_{\perp i}}, \\ (p_{ti})_\theta &= L_{ti} = 2ar_i^2 f(v_{\perp i}), \\ 4v_{\perp i} f(v_{\perp i}) &= \frac{\arcsin v_{\perp i}}{v_{\perp i}} - \frac{1}{\gamma_{\perp i}}, \end{aligned} \quad (4)$$

where $v_{\perp i}$ is the quark velocity perpendicular to \mathbf{r}_i . Making the substitution (2) we obtain

$$H_i = \sqrt{(\mathbf{p}_i - \mathbf{p}_{ti})^2 + m_i^2} + H_{ti}. \quad (5)$$

The square-root term can be reexpressed as

$$\begin{aligned} \sqrt{(\mathbf{p}_i - \mathbf{p}_{ti})^2 + m_i^2} &= \sqrt{W_{ri}^2 + \frac{p_{qi\theta}^2}{r_i^2}} \\ &\equiv W_{ri}\gamma_{\perp i}, \end{aligned} \quad (6)$$

where

$$\begin{aligned} W_{ri} &\equiv \sqrt{p_{ri}^2 + m_i^2}, \\ p_{qi\theta} &\equiv r_i W_{ri} v_{\perp i} \gamma_{\perp i}, \end{aligned} \quad (7)$$

and $\gamma_{\perp i}^{-2} \equiv 1 - v_{\perp i}^2$.

For a meson we must add contributions (5) for both quarks. To ensure that the meson is at rest we take $p_{r1} = p_{r2} = p_r$ and a separate constraint that the total momenta perpendicular to the rotation axis and to the interquark axis must vanish [2]. In two important special cases this latter constraint is trivially satisfied. For equal mass quarks the total perpendicular momentum clearly vanishes. For heavy-light mesons the constraint has no effect since the c.m. point always remains close to the heavy quark.

Summing (5)–(7) for both quarks yields, for an equal quark mass meson,

$$\frac{L}{r} = W_r \gamma_{\perp} v_{\perp} + ar f(v_{\perp}), \quad (8a)$$

$$H = 2W_r \gamma_{\perp} + ar \frac{\arcsin v_{\perp}}{v_{\perp}}, \quad (8b)$$

and for a heavy-light meson with the heavy quark mass $m_2 \gg m_1$ and $m_2 \gg ar$,

$$\frac{L}{r} = W_r \gamma_{\perp} v_{\perp} + 2ar f(v_{\perp}), \quad (9a)$$

$$H - m_2 = W_r \gamma_{\perp} + ar \frac{\arcsin v_{\perp}}{v_{\perp}}, \quad (9b)$$

where $f(v_{\perp})$ is defined in (4), W_r in (7), and $r = r_1 + r_2$ is the interquark separation.

As a point of comparison we first seek the *grast*, or minimum energy for fixed angular momentum, solutions of (8) and (9). The minimum H will be M , the meson

mass. Denoting $\frac{\partial H}{\partial r} \equiv H_{,r}$, etc., two equations follow from the *grast* condition:

$$\begin{aligned} L_{,r} &= 0, \\ H_{,r} &= 0. \end{aligned} \quad (10)$$

For the equal mass equations (8) direct evaluation of the above derivatives and the elimination of $v_{\perp,r}$ yields

$$2m(\gamma_{\perp} v_{\perp})^2 = ar. \quad (11)$$

Substituting this back into (8) we find that

$$\frac{aL}{m^2} = \gamma_{\perp}^4 v_{\perp}^2 \left(\arcsin v_{\perp} + \frac{v_{\perp}}{\gamma_{\perp}} \right), \quad (12)$$

$$\frac{M}{2m} = \gamma_{\perp}^2 v_{\perp} \left(\arcsin v_{\perp} + \frac{1}{\gamma_{\perp} v_{\perp}} \right).$$

In the limit of large L or small m , v_{\perp} approaches unity and it follows that

$$\frac{L}{M^2} = \frac{1}{2\pi a} \equiv \alpha'_{\text{Nambu}}, \quad (13)$$

which is the well-known Nambu-Regge slope relation.

A similar *grast* solution for the heavy-light meson yields

$$\frac{aL}{m_1^2} = \frac{\gamma_{\perp}^4 v_{\perp}^2}{2} \left(\arcsin v_{\perp} + \frac{v_{\perp}}{\gamma_{\perp}} \right), \quad (14)$$

$$\frac{M - m_2}{m_1} = \gamma_{\perp}^2 v_{\perp} \left(\arcsin v_{\perp} + \frac{1}{\gamma_{\perp} v_{\perp}} \right).$$

The analogous Regge plot relation for the heavy-light case in the limit of large L or small m_1 is

$$\frac{L}{(M - m_2)^2} = \frac{1}{\pi a} = 2\alpha'_{\text{Nambu}}. \quad (15)$$

We note that the *grast* slope for heavy-light mesons is double the “Nambu” slope of (13).

For large angular momentum we expect correspondence between the *grast* and quantum solutions. It will be informative therefore to compare the results of the following two sections to the *grast* slopes of (13) and (15).

III. QUANTUM SOLUTION

From (8) or (9) the quantized solution would be relatively simple to construct if one could solve the angular momentum equation for v_{\perp} and substitute in the Hamiltonian. The resulting wave equation $H\psi(\mathbf{r}) = M\psi(\mathbf{r})$ could then be solved by standard numerical methods with the replacements $L^2 = \ell(\ell + 1)$ and $p_r^2 = -\frac{1}{r} \frac{\partial^2 r}{\partial r^2}$. Unfortunately, this is only feasible for heavy quarks in which case the Schrödinger equation with static linear confinement results [1].

Since we are faced with transcendental functions in (8a) or (9a) we must devise a numerical way to elimi-

nate v_\perp while treating v_\perp , r , and W_r as noncommuting operators. For definiteness we concentrate on the equal mass case. The heavy-light solution proceeds in a nearly identical way.

In our scheme we first reduce (8) to finite matrix equations by introducing a complete set of basis states $\{e_k(\mathbf{r})\}$ and then truncating at a finite number N :

$$\psi(\mathbf{r}) \simeq \sum_{k=1}^N c_k e_k(\mathbf{r}). \quad (16)$$

The spirit of this approximation parallels the well-known Galerkin method [8]. The basis set we work with is a variant of hydrogenic wave functions corresponding to a totally discrete energy spectrum [9]. Other convenient sets such as the spherical harmonic oscillator wave functions would presumably also suffice. As discussed further in the Appendix, the basis set contains a scale parameter β . We will show that the eigenvalues found are independent of β for a sufficiently large N . The larger the number N of basis states used, the wider the range of β for stability of the eigenvalues. Equation (8) can be thought of as two $N \times N$ matrix equations involving known r and W_r matrices and an unknown v_\perp matrix.

The second step is to solve (8a) for the v_\perp matrix. Since various functions of v_\perp enter, it is best to pick a direction in the basis function space in which v_\perp is diagonalized. The condition for finding such a direction is

$$\det \left[\frac{L}{r} - W_r \gamma_\perp v_\perp - a r f(v_\perp) \right] = 0, \quad (17)$$

where here by assumption v_\perp is a simple number. For N basis functions there are N zeros of the determinant. The matrices p_r^2 , $1/r$, and r are given in the Appendix in analytic form. As an example, we assume that $a = 0.2 \text{ GeV}^2$, $m = 0$, and $\beta = 1 \text{ GeV}$. The eigenvalues of v_\perp are the zeros of (17) and are exhibited in Fig. 2. From

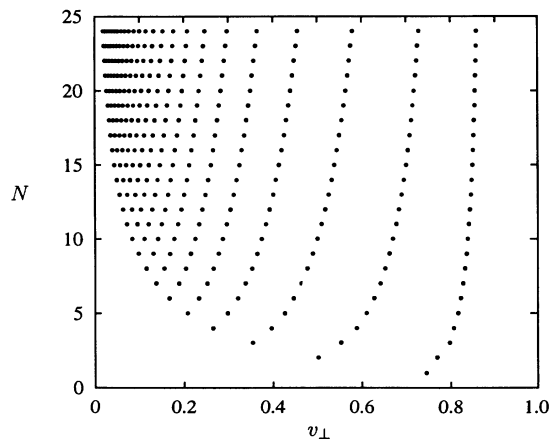


FIG. 2. Eigenvalues of v_\perp from the zeros of (17) with $\ell = 1$. For N basis states, N zeros, denoted by dots, are found. The eigenvalues lie between zero and unity and approach asymptotic values at large N . The zero distribution pattern shown corresponds to basis state scale $\beta = 1 \text{ GeV}$.

this figure we see that the eigenvalues of v_\perp are monotonically distributed between zero and unity, and evolve smoothly toward a limiting distribution as N becomes large. The matrix representation of v_\perp is then obtained by the inverse of the similarity transformation which diagonalizes v_\perp . The representation of v_\perp in the original basis set in general will be asymmetric and the similarity matrix will not be orthogonal. Any function of v_\perp can now be found in matrix form since the same similarity transformation diagonalizes any function of v_\perp .

The third and final step consists of substituting the matrix functions γ_\perp and $\arcsin v_\perp/v_\perp$ into the Hamiltonian. We then diagonalize H to obtain the eigenvalues, or meson masses, and the meson wave functions. If the v_\perp dependence appears in the same order in (8a) and (8b) the resulting Hamiltonian will be symmetric. It is clear that the same steps can be followed in the solution of (9) for heavy-light mesons.

In the following two sections we carry out the above procedure for equal mass quarks and for mesons composed of one heavy and one light quark.

IV. EQUAL MASS QUARKS

We now address the detailed solution of the coupled RFT equations (8) describing mesons composed of equal mass quarks. A short range, possibly Coulombic, interaction could easily be added to the Hamiltonian (8b) without changing the symmetry of the Hamiltonian or the calculational difficulty. For the most part we ignore such an addition in this paper except at the end of the next section on heavy-light mesons. In order to solve (8) we must specify the physical parameters, specifically the string tension a and the quark mass m . In the remainder of this paper we will assume that

$$a = 0.2 \text{ GeV}^2, \quad (18)$$

which is in agreement with most analyses of heavy quarkonia and yields a Nambu slope (13) $\alpha'_{\text{Nambu}} = (2\pi a)^{-1} = 0.8 \text{ GeV}^2$, which closely matches the universal Regge slope. We will in most cases plot our results in terms of a dimensionless mass $M^2/2\pi a$ so that the Regge slope should approach unity at large angular momentum and also the results can be scaled to any desired string tension. The remaining parameter is the quark mass for which we consider two illustrative cases.

A. Quark mass $m = 1.5 \text{ GeV}$

We first briefly discuss the results for two heavy quarks. The lowest-lying states are nearly nonrelativistic but as the angular momentum increases v_\perp approaches unity and the Regge structure should approach the massless case. The leading trajectory and three daughters are displayed in Fig. 3. The dots indicate the physical states which occur at integral angular momentum quantum number ℓ . The system of RFT equations (8) has been solved as a continuous function of orbital angular momentum as discussed in the Appendix. Since our solution is a continuous function of ℓ , it is straightforward to

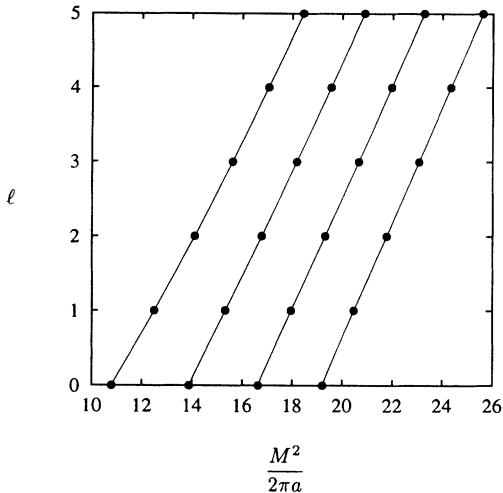


FIG. 3. Regge trajectory plot for heavy equal mass quarks $m = 1.5$ GeV. The leading trajectory and three daughter trajectories are shown. Equations (8) are solved for arbitrary ℓ and physical states are noted by dots at integral angular momentum quantum numbers.

compute the dimensionless Regge slope

$$\alpha' = 2\pi a \frac{d\ell}{dM^2}. \quad (19)$$

The slope of the four trajectories of Fig. 3 is shown in Fig. 4. We observe that for large angular momentum the slopes seem to approach unity as expected. The daughter trajectories approach the Nambu slope more slowly as might be anticipated since more energy is contained in radial motion.

B. Massless quarks ($m = 0$)

Nothing too unusual happens as the quark mass goes to zero. In Fig. 5 we show the leading and three daughter

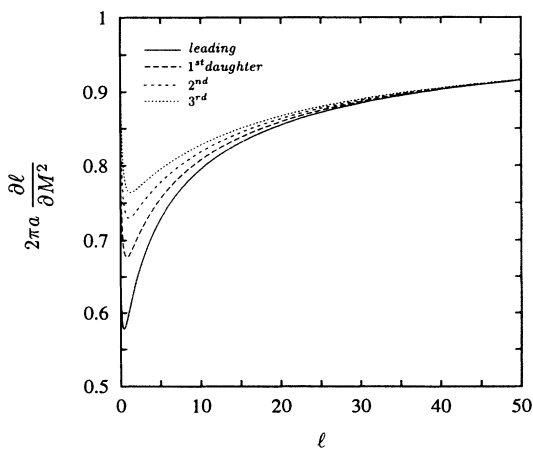


FIG. 4. Slope of $m = 1.5$ GeV trajectories of Fig. 3. The dimensionless slope of (19) is normalized so that the classical limit is unity. At large angular momentum the slope approaches the classical limit.

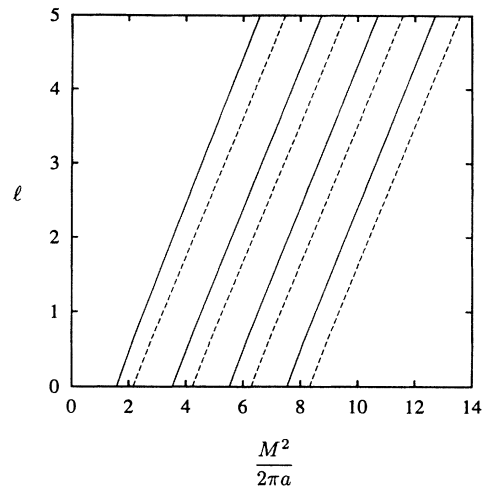


FIG. 5. Light quark Regge plot. The leading trajectory and three daughters are shown for $m = 0$ (solid line) and $m = 0.3$ GeV (dotted line).

trajectories for the cases of $m = 0$ (solid line) and $m = 0.3$ GeV (dashed line). The $m = 0.3$ GeV trajectories are displaced but otherwise similar. For these upper four $m = 0$ trajectories we compute the dimensionless slope (19) as shown in Fig. 6. We show in this figure results for $N = 15$. For $\ell = 40$ the slope of the leading trajectory still differs by a fraction of a percent from unity and the daughters by successively larger amounts.

The $N = 50$ solution is used in Fig. 7 to display the global structure of the RFT model particle spectrum for massless quarks. Again, the dots indicate physical states of integral orbital angular momentum.

From Fig. 7 we observe the following.

- (1) The trajectories are remarkably straight and evenly spaced.
- (2) The physical states align into towers of approximately mass-degenerate states of even or odd ℓ . For the

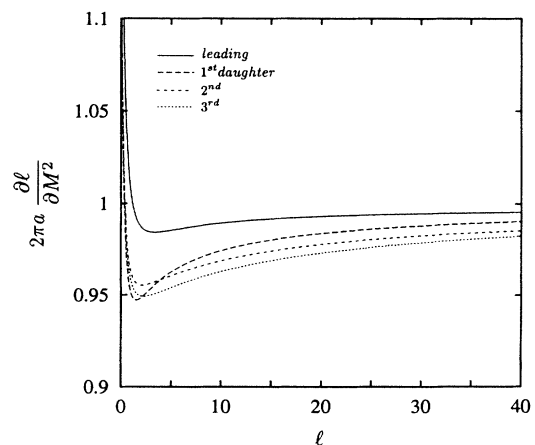


FIG. 6. Dimensionless slope for massless quarks showing convergence to unit slope at large ℓ . The classical limit is approached from below since radial oscillations add to the meson energy.

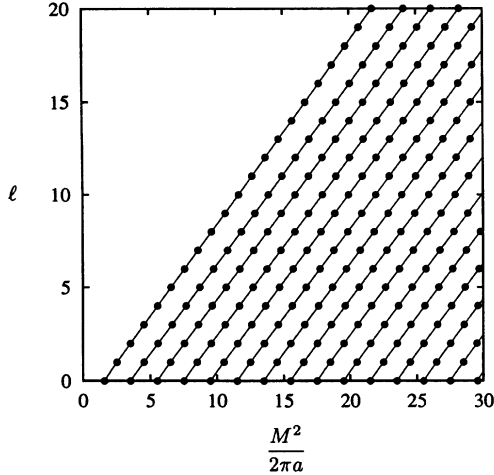


FIG. 7. Particle spectrum for massless quarks showing the Regge classification out to $\ell = 20$. The physical states are denoted by dots. The towerlike structure for even and odd ℓ should be noted. The solution shown used $N = 50$ basis states.

$\ell_{\max} = 2$ tower the $\ell = 0$ and $\ell = 2$ states are degenerate to within 1 MeV and for the $\ell_{\max} = 4$ tower the $\ell = 0, 2$, and 4 states are the same mass within 16 MeV. The lack of mass degeneracy becomes more pronounced for the higher towers; for example, the $\ell_{\max} = 15$ tower contains states separated by as much as 70 MeV.

Finally we refer the reader to the Appendix for a discussion of the convergence of our numerical eigenvalues as a function of trial function scale parameter β and number of basis states N . Our system of equations does not appear to fit the standard Galerkin theorem [8] requirements of a self-adjoint and positive definite eigenvalue equation. In this case we are assured that each eigenvalue approaches the correct one from above as a function of any variation such as β or N . In the RFT solution two nested eigenvalue problems are solved using the same basis states. One of these eigenvalue problems is a nonstandard one involving a nonorthogonal similarity transformation. (Despite this complication we see in Figs. 11–13 flat regions in β which widen as N increases. These β plots are very similar to those for a single wave equation in the potential model [10].)

V. HEAVY-LIGHT QUARK MESONS

Another interesting class of mesons is when one of the quarks (m_2) becomes very massive, specifically $m_2 \gg m_1$ and $m_2 \gg ar$. As seen in Sec. II the classical yrast solution (15) to the heavy-light equation (9) implies a Regge-type slope double the normal Nambu slope (13). To observe Regge behavior we must first subtract the heavy quark mass from the meson state mass before squaring.

The numerical solution of (9) proceeds similarly to the equal mass case. In Fig. 8 we exhibit the leading trajectory and three daughters for the limiting case $m_1 = 0$ and m_2 infinite. The angular momentum quantum number is plotted as a function of a dimensionless mass squared

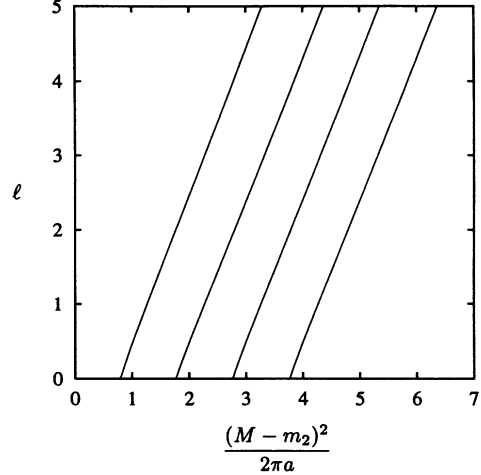


FIG. 8. Heavy-light Regge structure with $m_1 = 0$, m_2 infinite. The leading trajectory and three daughters are shown. Equations (9) were solved with $N = 15$.

$\frac{(M-m_2)^2}{2\pi a}$. Again we observe apparently straight evenly spaced trajectories but this time of dimensionless slope 2 as one would expect from the yrast solution (15). It is interesting to note that although the slope has changed the trajectory spacing compensates so that the tower mass degeneracy is preserved. The detailed structure can be seen from the slope plot of Fig. 9. As in the equal mass case the leading trajectory most rapidly approaches the classical solution, followed in turn by successive daughters as one would expect.

It is of interest to see if the actual heavy-light meson spectrum is consistent with the predicted doubling of the Nambu slope. Since we are presently considering spinless quarks, we should use the observed states to compute a spin-averaged spectrum. In Table I we show the heavy-light states which have established quark model spectroscopic assignments [11].

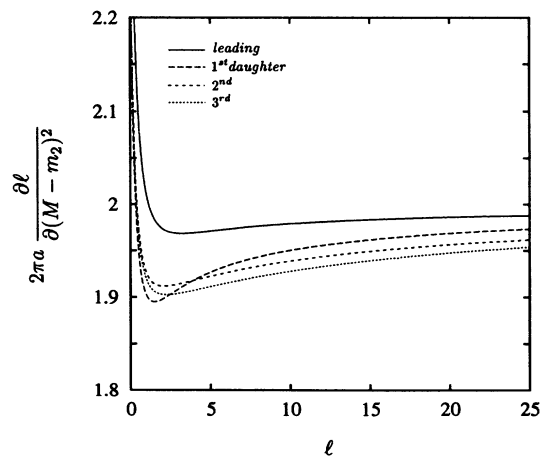


FIG. 9. Dimensionless slope for the heavy-light system of Fig. 8. The classical limit in this case is double the equal mass limit. Again the quantum solution approaches the classical limit from below due to radial motion in the quantized case.

TABLE I. Heavy-light spin-averaged states. Using ten observed heavy-light mesons having established quark spectroscopies [11] six spin-averaged levels can be extracted as discussed in the text. Using the RFT model with a Coulombic short-range part all of these levels are accounted for using standard values (20) for masses, string tension, and short range coupling.

State	Spectroscopic label J^P	$^{2S+1}L_J$	Spin-averaged mass (MeV)
<i>cū, cđ</i> quarks			
<i>D</i> (1867)	0^-	1S_0	1 <i>S</i> (1974)
<i>D*</i> (2009)	1^-	3S_1	
<i>D</i> ₁ (2424)	1^+	1P_1	1 <i>P</i> (2424)
<i>D*</i> ₂ (2459)	2^+	3P_2	
<i>cš</i> quarks			
<i>D_s</i> (1969)	0^-	1S_0	1 <i>S</i> (2075)
<i>D*</i> _s (2110)	1^-	3S_1	
<i>D_{s1}</i> (2537)	1^+	1P_1	1 <i>P</i> (2537)
<i>bū, bđ</i> quarks			
<i>B</i> (5279)	0^-	1S_0	1 <i>S</i> (5312)
<i>B*</i> (5325)	1^-	3S_1	
<i>bš</i> quarks			
<i>B_s</i> (5375)	0^-	1S_0	1 <i>S</i> (5416)

From Table I we note that the *cq̄* meson *s*-wave hyperfine splitting is about 140 MeV for both *cū* and *cš*, as expected by heavy quark symmetry. The *B** – *B* difference is about 50 MeV which follows if the color-magnetic moment of the heavy quark is inversely proportional to its mass. We therefore expect the *bš* *s*-wave hyperfine splitting to be about 50 MeV. The spin-averaged 1*S* state of *bš* may then be confidently predicted. Assuming the *p*-wave hyperfine splitting is small, we may take the observed *D*₁ and *D_{s1}* states as the two 1*P* spin-averaged states.

As a semirealistic model we add to the Hamiltonian (9b) a short range interaction $H_{SR} = -\kappa/r$. We fix the light quark mass at $m_\ell = 300$ MeV and the string tension $a = 0.2$ GeV². By varying the remaining parameters to the values

$$\begin{aligned} m_s &= 517 \text{ MeV}, \\ m_c &= 1285 \text{ MeV}, \\ m_b &= 4626 \text{ MeV}, \\ \kappa &= 0.51, \end{aligned} \quad (20)$$

we fit all six of the spin-averaged states of Table I exactly. These parameters are consistent with previous fits to spin-averaged *cĉ* and *bĉ* data [9]. The *D* and *D_s* leading trajectories generated by our fit are shown in Fig. 10. The four charm spin-averaged experimental states of Table I are shown by dots. The reader should be reminded that our calculation assumes that one of the quarks is very massive, which is not clearly valid for the charm quark.

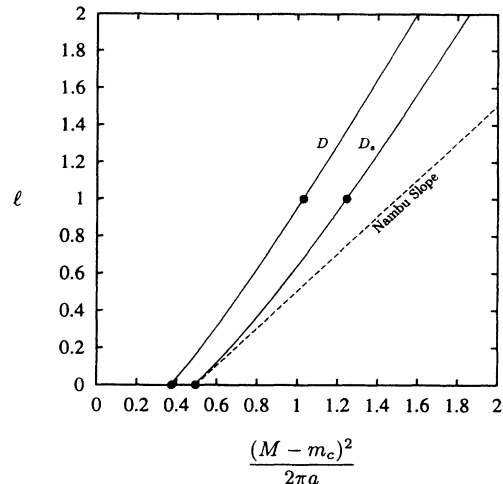


FIG. 10. *D* and *D_s* leading trajectories from the fit to the data of Table I. The four observed spin-averaged states are denoted by dots. The dashed line indicates the universal Regge slope for light quark states.

VI. SUMMARY AND CONCLUSIONS

The flux tube model has slowly evolved from a classical generalization of the QCD string [12], a unifying picture of many possible states of hadronic matter [13], and a simple physical explanation of the spin dependence expected in QCD [14] into a realistic successor to the potential model.

The potential model with scalar confinement has failed in several respects. It generates relativistic spin-independent corrections which are inconsistent with QCD and it behaves poorly in the limit of small quark mass [2]. Both of these shortcomings are circumvented within the RFT model [2, 3]. The main new ingredient in the RFT model is to include the angular momentum and rotational energy of the interacting field. In the potential model only the field energy is considered.

Of course any specific model such as the RFT model cannot compete with a fundamental QCD calculation. It is also clear that our understanding of QCD at this point does not permit wide ranging fundamental predictions in particle spectroscopy. The advantage of the potential model is that it is QCD motivated in the quasistatic (nonrelativistic) limit and is easy to solve. Once relativistic corrections are considered, the potential model unfortunately diverges from QCD. The RFT model can be considered as the simplest generalization of the potential model which retains the known properties of QCD for moving quarks. The drawback of the RFT model is that it is more difficult to solve.

Earlier [1] we addressed the question of the quantization of mesons consisting of relativistic spinless quarks joined by a straight flux tube or QCD string. The method used to solve these two transcendently coupled operator equations is essentially the same as in the present paper. The major change is the realization that the object of the solution is to eliminate v_\perp and that any method which respects the matrix nature of the variables will be equiv-

alent. A crucial step is that the transcendental matrix equations are reduced to algebraic ones if one works in a representation in which v_{\perp} is diagonal.

The method developed is applied to numerically solve mesonic systems with equal mass quarks and with one light and one heavy quark. In both cases a simple Regge spectrum emerges. For massless quarks, or for one heavy and one massless quark, we find a sensibly straight leading trajectory accompanied by an apparently infinite number of equally spaced daughter trajectories. For two massless quarks the Regge slope is the classical Nambu slope of $\alpha'_{\text{Nambu}} = (2\pi a)^{-1}$. For heavy-massless mesons a similar spectrum of states is found but with $\alpha' = 2\alpha_{\text{Nambu}}$.

Finally, we compare RFT predictions to the observed heavy-light mesons. After adding a short range Coulombic interaction to the heavy-light Hamiltonian we are able to account perfectly for the six known spin-averaged heavy-light states. The parameters of the fit (20) are quite consistent with those obtained in accounting for charmonium and bottomonium levels. It should be emphasized that m_c^{-1} corrections may well be appreciable, so that the parameters given in our fit (20) cannot be taken too seriously. A more rigorous test of the RFT model must allow for arbitrary masses as well as include fermionic quarks at the ends of the tube.

ACKNOWLEDGMENTS

This work was supported in part by the U.S. Department of Energy under Contract No. DE-AC02-

76ER00881 and in part by the University of Wisconsin Research Committee with funds granted by the Wisconsin Alumni Research Foundation.

APPENDIX: MATRIX REPRESENTATIONS AND CONVERGENCE OF ENERGY EIGENVALUES

The radial basis functions are those used in previous calculations [9, 10]: namely,

$$R_i^l(r) = N_{il}\beta^{3/2}(2\beta r)^l e^{-\beta r} L_i^\alpha(2\beta r), \quad (\text{A1})$$

where

$$N_{il}^2 = \frac{8(i!)}{\Gamma(i + \alpha + 1)} \quad (\text{A2})$$

and

$$\alpha = 2l + 2 \quad (\text{A3})$$

and it assumed that $0 \leq i \leq N - 1$. For computational precision and efficiency, the matrix representation of all operators (with the exception of v_{\perp}) has been calculated analytically. These expressions have also been extended to nonintegral l for the purpose of computing Regge trajectories and slopes thereof. For example,

$$p_r^2 = -\frac{1}{r} \frac{\partial^2}{\partial r^2} r \quad (\text{A4})$$

can be computed analytically. The result is (for $i \leq j$)

$$\begin{aligned} \langle p_r^2 \rangle_{ij} = & -\frac{\beta^2}{2} N_{il} N_{jl} \left\{ \frac{(i + \alpha)!}{i!} \left[(j - i)(1 - \delta_{i,j-1} - \delta_{ij}) + \delta_{i,j-1} + \frac{1}{4} \delta_{ij} \right] \right. \\ & \left. + \sum_{k=0}^i \frac{(k + \alpha - 1)!}{k!} \left[-\alpha(j - k) - \frac{\alpha}{2} + \left(\frac{l(l+1)(i+1-k)(j+1-k)}{k + \alpha - 1} \right) \right] \right\}. \end{aligned} \quad (\text{A5})$$

To compute the W_r matrix we use (A5) to obtain $W_r^2 = p_r^2 + m^2$ and then the matrix square root. This is done by diagonalizing W_r^2 , taking the square root of the diagonal elements, and then rotating back to obtain the W_r matrix. The other analytic expressions used are (for $i \leq j$) [10]

$$\left\langle \frac{1}{r} \right\rangle_{ij} = \frac{\beta}{4} N_{il} N_{jl} \sum_{k=0}^i \frac{(k + \alpha - 1)!}{k!} \quad (\text{A6})$$

and

$$\begin{aligned} \langle r \rangle_{ij} = & \frac{1}{2\beta} \left[(2i + \alpha + 1)\delta_{i,j} - \sqrt{j(j + \alpha)}\delta_{i,j-1} \right. \\ & \left. - \sqrt{i(i + \alpha)}\delta_{i,j+1} \right], \end{aligned} \quad (\text{A7})$$

where results for $i > j$ are obtained by simple reflection

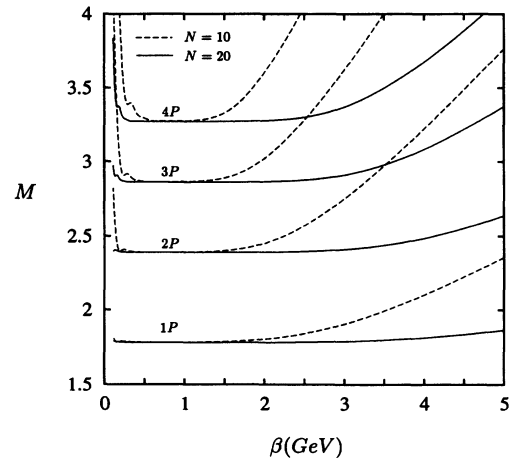


FIG. 11. Basis state scale parameter β dependence for the four lowest energy p -wave eigenvalues for massless quarks. As the basis state number N increases a clear region of convergence develops.

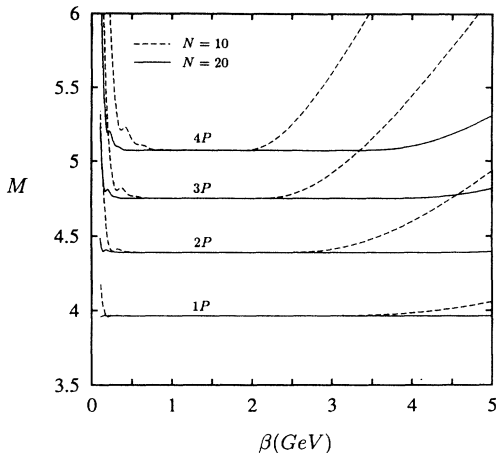


FIG. 12. Basic state scale parameter β dependence for the four lowest energy p -wave eigenvalues for two $m = 1.5$ GeV quarks.

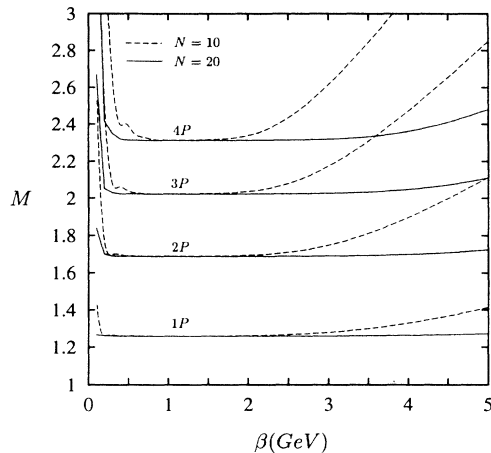


FIG. 13. Heavy-light meson basis scale β dependence for the four lowest p -wave eigenvalues.

due to the symmetry of the operators. For nonintegral l the factorials are replaced by the corresponding Γ functions and ratios of Γ functions are computed from the differences of their natural logarithms.

Figures 11 and 12 show the four lowest energy p -wave

eigenvalues for equal mass mesons as a function of the scale parameter, β , for $m_q = 0$ and $m_q = 1.5$, respectively. Figure 13 is the corresponding plot for $m_1 = 0$ and $m_2 = \infty$. In each instance increasing the number of basis states N enlarges the region of β where the eigenvalue is stable.

-
- [1] Dan LaCourse and M. G. Olsson, Phys. Rev. D **39**, 2751 (1989).
- [2] Collin Olson, M. G. Olsson, and Ken Williams, Phys. Rev. D **45**, 4307 (1992).
- [3] M. G. Olsson and Ken Williams, Phys. Rev. D **48**, 417 (1993).
- [4] N. Brambilla and G. M. Prosperi, Phys. Lett. B **236**, 69 (1990).
- [5] Alan Gara, Bernice Durand, and Loyal Durand, Phys. Rev. D **40**, 843 (1989).
- [6] A. B. Henriques, B. H. Keller, and R. G. Moorhouse, Phys. Lett. **64B**, 85 (1976); Lai-Him Chan, *ibid.* **71B**, 422 (1977); C. E. Carlson and Franz Gross, *ibid.* **74B**, 404 (1978); N. Isgur and G. Karl, Phys. Rev. D **18**, 4187 (1979); H. J. Schnitzer, Phys. Lett. **76B**, 461 (1978); Phys. Rev. D **18**, 3482 (1978).
- [7] E. Eichten and F. Feinberg, Phys. Rev. D **23**, 2724 (1981); D. Gromes, Z. Phys. C **22**, 265 (1984); **26**, 401 (1984); A. Barchielli, N. Brambilla, and G. M. Prosperi, Nuovo Cimento A **103**, 59 (1989); A. Barchielli, E. Montaldi, and G. M. Prosperi, Nucl. Phys. **B296**, 625 (1988); **B303**, 752(E) (1988).
- [8] I. Stakgold, *Green's Functions and Boundary Value Problems* (Wiley, New York, 1984).
- [9] S. Jacobs, M. G. Olsson, and C. J. Suchyta III, Phys. Rev. D **33**, 3338 (1986).
- [10] Lewis P. Fulcher, Zheng Chen, and K. C. Yeong, Phys. Rev. D **47**, 4122 (1993).
- [11] Particle Data Group, K. Hikasa *et al.*, Phys. Rev. D **45**, S1 (1992). The B_s (5375) has been observed by the ALEPH detector at LEP [S. L. Wu, Bull. Am. Phys. Soc. **38**, 922 (1993)].
- [12] A. Chodos and C. B. Thorn, Nucl. Phys. **B72**, 509 (1974); I. Bars, *ibid.* **B111**, 413 (1976); M. Ida, Prog. Theor. Phys. **59**, 1661 (1978).
- [13] N. Isgur and J. Paton, Phys. Rev. D **31**, 2910 (1985); Phys. Lett. **124B**, 247 (1983).
- [14] W. Buchmüller, Phys. Lett. **112B**, 479 (1982).